# Direct inversion of shallow-water bathymetry from EO-1 hyperspectral remote sensing data

**Zhishen Liu (刘智深) and Yan Zhou (周 燕)***

*Ocean Remote Sensing Institute, Ocean University of China, Qingdao 266003, China*

**Corresponding author: kexinyan0317@163.com*

Received November 5, 2010; accepted January 28, 2011; posted online May 12, 2011

Using the US National Aeronautics and space Administration (NASA) Earth Observing-1 Mission (EO-1) hyperion hyperspectral remote sensing data, we study the shallow-water bathymetry inversion in Smith Island Bay. The fast line-of-sight atmospheric analysis of spectral hypercubes module is applied for atmospheric correction, and principal component analysis method combined with scatter diagram and maximum likelihood classification is used for seabed classification. The diffuse attenuation coefficient $K_{\rm d}$ is derived using quasi-analytical algorithm (QAA), which performs well in optically deep water. $K_{\rm d}$ obtained from QAA requires correction, particularly those derived in some coastal areas with optically shallow water and calculated by direct inversion based on radiative transfer theory to obtain the bathymetry. The direct inversion method derives the water depth quickly, and matches the results from optimized algorithm.

*OCIS codes:* 010.0280, 280.1355.

*doi: 10.3788/COL201109.060102.*

Shallow-water bathymetry, traditionally obtained using acoustic sonar, has been playing a significant role in military, commercial, and recreational activities. However, bathymetry data cannot be obtained by sonar or updated in time in some coastal areas that are not accessible to ships. Effective ways of obtaining shallow-water bathymetry data quickly and accurately have yet to be discovered.

Scientists have been conducting research on the retrieval of shallow-water bathymetry for many years. In 1969, scientists from the Michigan Environment Research Center retrieved bathymetry using the multispectral remote sensing data[1]. In 1993, Hamilton *et al.* retrieved bathymetry by analyzing the regression relationship between on-spot data and bathymetry data with the experimental model, which can only be applied in particular areas[2]. Different surveying data have been used for the statistical regress according to types of remote sensing data. Sandidge *et al.* retrieved shallow-water bathymetry by neural network, which required surveying data to set up a training group[3]. Lee *et al.* retrieved bathymetry using the AVIRIS data through semi-analysis model and optimization algorithm[4]. Satellite data have been widely used in remote sensing retrieval[5]. Lee *et al.* used hyperion data to develop and test optimization algorithm[6]. Direct inversion based on radiative transfer theory is introduced in this letter to obtain bathymetry in coastal areas.

The US National Aeronautics and Space Administration (NASA) Earth Observing-1 Mission (EO-1) hyperion data are used in this letter. Hyperion is a hyperspectral sensor that has 220 spectral bands, with wavelengths from 0.4 to 2.5 $\mu$m, 10-nm spectrum resolution, and 30-m spatial resolution[7]. In this letter, level 1 data are used and located in the Smith Island Bay, a part of Chesapeake Bay, America, which is shown in Fig. 1. Its costal seabed is a continental shelf. The data provided by the US Geological Survey (USGS) were collected on August 28, 2004 (37.476°N 75.779°W). Only spectral information in the range of 428–925 nm was used because our work focused on the bottom properties.

Diminishing the influence of the atmosphere is a critical pre-processing step, and the fast line-of-sight atmospheric analysis of spectral hypercubes (FLAASH)[8] module is used for atmospheric correction. It's a part of the remote sensing data processing software ENVI and capable of retrieving spectral reflectance from hyperspectral radiance images. It contains the MODTRAN4 radiation transfer code. We may choose any of the standard MODTRAN model atmospheres and aerosol types to represent the scene, and a unique MODTRAN solution is computed for each image.

Since clouding in remote sensing images is the minimal, we do not remove clouding in this letter[9,10]. After atmosphere correction, some pixel spectra produce zigzag noise, which can be eliminated by minimum noise fraction. This method does not reduce the image spatial resolution. It shows several spectra after the atmospheric correction and spectral optimization (Fig. 2). Each spectrum curve corresponds to a 30×30 (m) pixel.

Based on the radiative transfer theory and following the method of Gianinetto *et al.*[11,12], the radiative transfer equation for light in the water is

$$L_{\rm w} = T_{\rm w} L_{\rm s} + (1 - T_{\rm w}) L_{\rm dw}, \tag{1}$$

Fig. 1. Hyperion collection (August 28, 2004) over the Chesapeake Bay. Left is the full scene; right is a subset located in Smith Island.

 

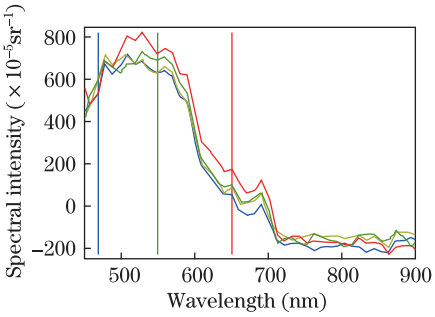


Fig. 2. Spectrum after correction of atmospheric effects by FLAASH module and spetral optimization.

where $L_{\rm w}$ is the water-leaving radiance, $L_{\rm s}$ is the bottom radiance, $L_{\rm dw}$ is the reflected radiance from the water, and $T_{\rm w}$ is the transmittance of the water body and can be expressed as

$$T_{\rm w} = {\rm e}^{-2K_{\rm d}z}. \tag{2}$$

According to Eqs. (1) and (2), the radiative transfer equation can be expressed as

$$L_{\rm w} = L_{\rm dw} + (L_{\rm s} - L_{\rm dw}){\rm e}^{-2K_{\rm d}z}. \tag{3}$$

Equation (3) can be expressed in the form of reflectance as

$$R_{{\rm w}i}(\lambda) = R_{{\rm dw}i}(\lambda) + R_{{\rm s}i}(\lambda) - R_{{\rm dw}i}(\lambda){\rm e}^{-2K_{{\rm d}i}(\lambda)z}. \tag{4}$$

The bathymetry can be solved using Eq. (4), which is expressed as

$$z = \sum\nolimits_{i=1}^{N} \frac{\ln[R_{{\rm w}i}(\lambda) - R_{{\rm dw}i}(\lambda)]/[R_{{\rm s}i}(\lambda) - R_{{\rm dw}i}(\lambda)]}{-2K_{{\rm d}i}(\lambda)N}, \tag{5}$$

where $N$ is the number of wavelengths involved in bathymetry retrieval. This method can be applied to clear water, in which properties of bottom materials over the scene are known. It is unlikely to be true for many other coastal regions where variations in factors, such as suspended sediment, are an important consideration. Multispectral scanners with high spectral resolution should be utilized when visible and near-infrared bands could be used to separate substrate and water-column parameters. When sea surface reflectance, bottom albedo, and diffuse attenuation coefficient are obtained, the bathymetry is retrieved. The major steps of the computer algorithm that obtains water depth is shown in Fig. 3.

Principal component analysis method is employed for bottom classification. After the principal component transforms, the hyperspectral data of the regions of interests (ROIs) are integrated into the first several principal component wave bands, which have most information of scene. Subsequently, the selected bands are taken into $n$-dimensional visualizing tool in ENVI to obtain $n$-dimensional space scatter plot. Interesting types are selected by spectral clustering and inputted into ROI tools. The bottom is classified by maximum likelihood classification of ROI. Different bottom reflectance is adopted for bathymetry retrieval according to different bottom types.

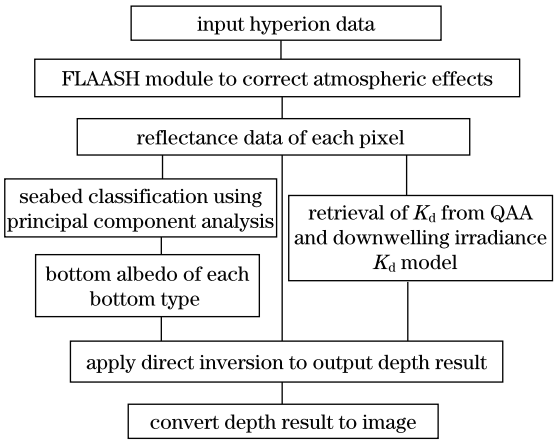


Fig. 3. Major steps of the computer algorithm that obtains water depth.

To emphasize the properties of optically shallow water, pixels of land are masked as black. After principal component transformation, we select the first eight principal component wave bands. To find interesting end members effectively, we select the principal component bands 1, 2, and 7 for the $n$-dimensional visualizing tool and obtained three-dimensional (3D) space scatter plot, as shown in Fig. 4(a). Through spectral clustering and maximum classification, the seabed is classified into three types (Fig. 4(b)).

Generally, seabed substrate can be divided into the silt, rock type, and the plant type (e.g., each kind of algae's seabed). There is considerable reflectance spectrum difference between two kinds of seabed. Silt-type seabed reflectance spectrum is progressively increasing and fluctuations are not large compared with the reflectance spectrum fluctuations of plant-type seabed, which are significantly larger. Considering sandy-type bottom as the dominant bottom substrate through numerous experiments and based on the general condition of seabed, we classify the seabed into three types: silt bottom, sand bottom, and optically deep water. Coral-colored areas are identified as silt bottom and selected near-shore remote sensing reflectance is the bottom albedo, as shown in Fig. 5. Cyan-colored areas are classified as sand bottom and selected remote sensing reflectance spectra of sand bottom are seen through clear water at depth of 0.1 m, which are simulated using Hydrolight taken by Philpot *et al.* (2004)[13]. Blue-colored areas are classified as optically deep water areas which do not consider bottom reflectance.

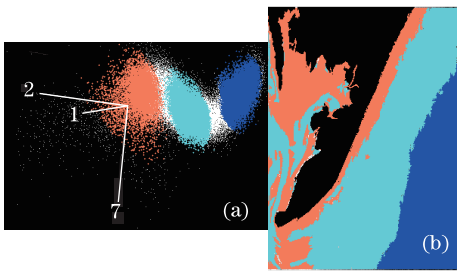


Fig. 4. (a) 3D space scatter plot of principal component bands 1, 2, and 7; (b) result of seabed classification.

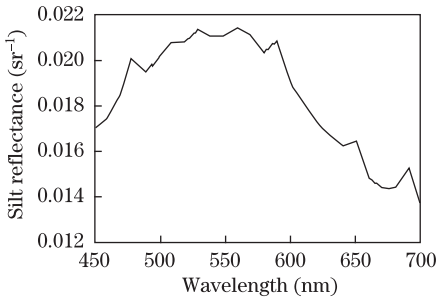


Fig. 5. Silt bottom albedo spectrum.

In ocean remote sensing, the downward diffuse attenuation coefficient $K_{\rm d}$ is an important parameter used in the bathymetry retrieval. In ocean optics, $K_{\rm d}$ at a certain depth $z$ is expressed as

$$K_{\rm d}(z) = -\frac{1}{E_{\rm d}(z)}\frac{{\rm d}E_{\rm d}(z)}{{\rm d}z}. \tag{6}$$

Lee *et al.* expressed the downward diffuse attenuation coefficient as follows according to the analysis and simulation of the radiative transfer equation in water[14]:

$$K_{\rm d} = m_0 a + \upsilon b_{\rm b}, \tag{7}$$

where $m_0$ and $\upsilon$ account for the contribution of the absorption and the backscattering of the water,

$$m_0 \approx 1 + 0.005\,\theta_{\rm a}, \tag{8}$$

$$\upsilon = m_1(1 - m_2 {\rm e}^{-m_3 a}), \tag{9}$$

where $\theta_{\rm a}$ is the solar zenith above the sea surface. The values of the four model parameters $m_0$, $m_1$, $m_2$, and $m_3$ are needed for the desired solar altitude and depth.

According to the quasi-analytical algorithm (QAA) of Lee *et al.*[15], the absorption coefficient $a$ and the backscattering coefficient $b_{\rm b}$ can be retrieved by the remote sensing reflectance. Subsequently, the downward diffuse attenuation coefficient can be retrieved by $a$, $b_{\rm b}$, and Eq. (7). This method can be applied in optically deep water. However, many coastal areas exist with considerable optically shallow water. Thus, the $K_{\rm d}$ obtained should be corrected.

Assuming that the sea bottom depth is $z$, the downward irradiance of sea surface is $E_{\rm d}(0)$, and the transmittance of the optical deep water body is $T(z)$, then the irradiance through the sea bottom is $E_{\rm d}(0)T(z)$ and $E_{\rm d}(0)T(z)r$ is reflected by sea bottom, which is the upward irradiance contribution quantity. $E_{\rm d}(0)T(z)rR(z)$ is reflected by water column and becomes the downward irradiance contribution quantity. After unlimited back and forth reflections, the downward irradiance of sea bottom can be expressed as

$$\begin{aligned} E_{\rm d} &= E_{\rm d}(0)T(z) + E_{\rm d}(0)T(z)rR(z) + \cdots \\ &= E_{\rm d}(0)T(z)\sum_{n=0}^{\infty}\Big[rR(z)\Big]^n \\ &= E_{\rm d}(0)T(z)\Big[\frac{1}{1-rR(z)}\Big]. \end{aligned} \tag{10}$$

$K_{\rm d}$ between depth of zero and depth $z$ can be expressed as

$$K_{\rm d}(z) = -\frac{1}{z}\ln\Big[\frac{E_{\rm d}(z)}{E_{\rm d}(0)}\Big]. \tag{11}$$

According to Eqs. (10) and (11), the downward diffuse attenuation coefficient of optically shallow water $K_{\rm ds}(z)$ can be expressed as

$$K_{\rm ds}(z) = K_{\rm d}(z) + \frac{1}{z}\ln[1 - rR(z)]. \tag{12}$$

The downward diffuse attenuation coefficient of infinitely deep water $K_{\rm d}$ can be derived from QAA. The bottom albedo $r$ can be obtained from analysis of sea bottom types. $R(z)$ is approximated to the reflectance of sea surface, which is $\pi$ times the value of remote sensing reflectance in isotropic radiation field. However, $K_{\rm ds}$ remains related with the depth $z$ of the second item on the right of Eq. (12). We factor the downward diffuse attenuation coefficient of infinitely deep water $K_{\rm d}$ into the direct inversion method to obtain depth $z$ and complete $K_{\rm ds}1$ first-level approximation, and then use $K_{\rm ds}1$ to extract the second-level approximation $K_{\rm ds}2$. Thus, further approximation calculation should be carried out to obtain the true value of $K_{\rm ds}$. The computed result indicates that such circulation computation converged quickly.

In this letter, the downward diffuse attenuation coefficient of finite water $K_{\rm ds}$ selects the first-level approximation $K_{\rm ds}1$. The result is shown in Fig. 6.

According to the above-mentioned method, the result from the bathymetry should be compared with that of spectral optimization approach developed by Lee *et al.*[16] The comparative result is shown in Fig. 7. Spatially, a parallel pattern to the coastal line shown from offshore to onshore is seen.

The spectral optimization approach analytically models $R_{\rm rs}$ spectrum as a function of five independent variables, representing properties of water column and bottom, for optically shallow water. Multiple bottom types could be incorporated into the semi-analytical model but it is only the spectral reflectance shape of a sandy-type bottom that we consider as it is the dominant bottom substrate. By varying the values of the five unknowns, they are considered derived when the modeled $R_{\rm rs}$ spectrum best matches the hyperion $R_{\rm rs}$ spectrum. It derives all the constituents from the imagery, thus direct inversion result is compared with the result of spectral optimization approach.

We select one of the deep water regions A and one of the shallow water regions B in Fig. 7(a) and compare the

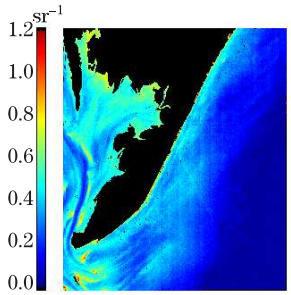


Fig. 6. Retrieved diffuse attenuation coefficient $K_{\rm d}(555)$ after correction.

result derived from two methods. The results of the comparison are given in Figs. 8 and 9, which show that the retrieved bathymetry value is close to the optimized value. Mean relative differences of deep water region A and shallow water region B are 12.12% and 20.89%, respectively. Specifically, it is approximately 1 m for deep water regions and 0.2 m for shallow water regions. They have the same trend from the shallower water to the deeper water.

In conclusion, we introduce a direct inversion method based on radiative transfer theory to obtain the shallow-water bathymetry using the hyperspectral remote sensing data in Smith Island Bay. The FLAASH module is used to perform atmospheric correction and the principal component analysis for seabed classification. After the atmospheric correction, the diffuse attenuation coefficient of the sea water, bottom classification, and bathymetry are retrieved data in Smith Island Bay. The FLAASH module is used to perform atmospheric correction and the principal component analysis for seabed classification. After the atmospheric correction, the diffuse attenuation coefficient of the sea water, bottom classification, and bathymetry are retrieved transfer theory. We compare the retrieved results with the optimized results and verify the rationality of the bathymetry retrieval method as well as the validity of principal component analysis for seabed

This work was supported by the Key Funds Program of the National Natural Science of China under Grant No. 60638020.

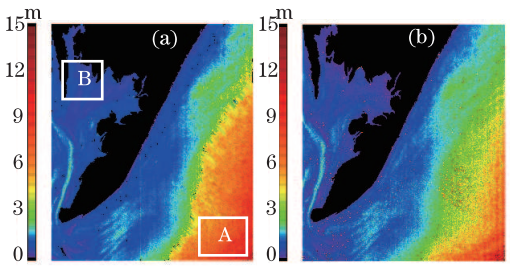


Fig. 7. (a) Result of the bathymetry derived from radiative transfer; (b) result of the bathymetry derived from spectral optimization.

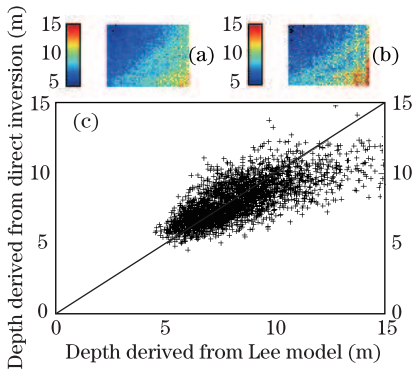


Fig. 8. Comparison of deep water region A. (a) Radiative transfer inversion result image; (b) spectral optimization result image; (c) comparison of depth between direct inversion result and optimized result in panels a and b.

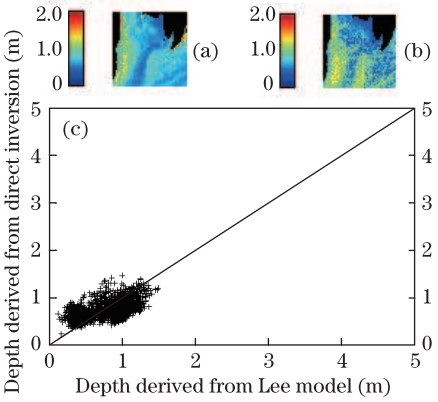


Fig. 9. Comparison of shallow water region B. (a) Radiative transfer inversion result image; (b) spectral optimization result image; (c) comparison of depth between direct inversion result and optimized result in panels a and b.

classification.

## References

1. F. C. Polcyn and D. R. Lyzenga, in *Proceedings of Symposium of Signif icant Results from ERTS-1* 1433 (1973).
2. M. K. Hamilton, C. O. Davis, W. J. Rhea, S. H. Pilorz, J. M. Paredes, and K. L. Carder, Remote Sens. Environ. **44,** 217 (1993).
3. J. C. Sandidge and R. J. Holyer, Remote Sens. Environ. **65,** 341 (1998).
4. Z. Lee, K. L. Carder, R. F. Chen, and T. G. Peacock, J. Geophys. Res. **106,** 11639 (2001).
5. T. Cui, J. Zhang, J. Tang, Y. Ma, and S. Qing, Chin. Opt. Lett. **8,** 721 (2010).
6. Z. P. Lee, B. Casey, R. Arnone, A. Weidemann, R. Parsons, M. J. Montes, B.-C. Gao, W. Goode, C. O. Davis, and J. Dye, J. Appl. Remote Sensing **1,** 011502 (2007).
7. D. L. B. Jupp and B. Datt, "Evaluation of the EO-1 hyperion hyperspectral instrument and its applications at Australian validation sites 2001-2003" CSIRO Earth Observation Centre Report (June, 2004).
8. Research Systems, Inc., *FLAASH Module User's Guide* (Version 4.2) (August, 2005).
9. X. Jiang, J. Lu, and W. Shen, Acta Opt. Sin. (in Chinese) **29,** (s1) 111 (2009).
10. X. Jiang, L. Dai, and W. Shen, Acta Opt. Sin. (in Chinese) **29,** (s1) 115 (2009).
11. M. Gianinetto and G. Lechi, International Archives of the Photogrammetry, Remote Sensing and Spatial Information Sciences **35,** (Part B) 94 (2004).
12. P. N. Bierwirth, T. J. Lee, and R. V. Burne, Photogramm. Eng. Remote Sensing **59,** 331 (1993).
13. W. Philpot, C. O. Davis, W. P. Bissett, C. D. Mobley, D. D. R. Kohler, Z. Lee, J. Bowles, R. G . Steward, Y. Agrawal, J. Trowbridge, R. W. Gould, Jr., and R. A. Arnone, Oceanography **17,** 77 (2004).
14. Z.-P. Lee, K.-P. Du, and R. Arnone, J. Geophys. Res. **110,** C02016 (2005).
15. Z. P. Lee, K. L. Carder, and R. Arnone, Appl. Opt. **41,** 5755 (2002).
16. Z. Lee, K. L. Carder, C. D. Mobley, R. G. Steward, and J. S. Patch, Appl. Opt. **38,** 3831 (1999).